

29th AIAA Aeroacoustics Conference, May 5-7 2008, Vancouver B.C.

# Numerical and Experimental Investigations of the Noise Generated by a Flap in a Simplified HVAC Duct

Anke Jäger<sup>1</sup>, Friedhelm Decker<sup>3</sup>, Michael Hartmann<sup>2</sup>,

Moni Islam<sup>3</sup>, Timo Lemke<sup>4</sup>, Jörg Ocker<sup>4</sup>, Volker Schwarz<sup>1</sup>, Frank Ullrich<sup>5</sup>,

Bernd Crouse<sup>6</sup>, Gana Balasubramanian<sup>6</sup>, Fred Mendonca<sup>7</sup> and Roger Drobietz<sup>8</sup>

This paper describes an investigation carried out by a consortium of the German car manufacturers Audi, BMW, Daimler, Porsche and Volkswagen of the feasibility of predicting the aerodynamically generated noise within an HVAC system by means of CFD (Computational Fluid Dynamics) and CAA (Computational Aeroacoustics). After a short introduction where the motivation for this study is described, the setup of an experiment specially designed for the validation of unsteady CFD and CAA calculations within HVAC systems is shown in detail. The model chosen for this validation study is a simplified HVAC duct that consists of a 90 degree bend with a rectangular cross section. Two different geometric variants of this HVAC duct are studied: One with a flap inside and one without a flap. Fluid dynamic as well as aeroacoustic investigations with this model in the two configurations are carried out in a specially designed test bench applying measurements of the mean flow quantities with PIV (Particle Image Velocimetry) as well as measurements of unsteady wall pressure fluctuations with microphones mounted flush to the duct surface. In the next section the numerical simulations conducted are discussed. As a first step of a CAA calculation, unsteady CFD calculations were conducted using two different commercial CFD codes, a finite volume code (STAR-CD) and a lattice Boltzmann code (PowerFLOW). The different methodologies of the two codes are briefly outlined. Then the numerical results are shown in detail and compared to the PIV as well as the unsteady wall pressure measurements. The comparison shows a good overall agreement of the numerical results obtained with the two codes for the time averaged flow structures as well as the time dependent flow phenomena. Slight differences between the two codes can be found concerning mainly the time averaged flow field. At the end of the paper further activities of the consortium are described including a validation study for the second step of a CAA calculation in HVAC systems consisting of the propagation of the aerodynamically generated sound to the passengers ears.

---

<sup>1</sup> Daimler AG, HPC X715, D-71059 Sindelfingen, Germany

<sup>2</sup> Volkswagen AG, Letterbox 1777, D-38436 Wolfsburg, Germany

<sup>3</sup> Audi AG, Wind-Tunnel Center, D-85045 Ingolstadt, Germany

<sup>4</sup> Dr.-Ing. h.c. F. Porsche AG, D-71286 Weissach, Germany

<sup>5</sup> BMW AG, Dept. EG-42, D-80788 Munich, Germany

<sup>6</sup> Exa Corporation, 150 North Hill Drive, Brisbane, CA 94005, USA

<sup>7</sup> CD-adapco UK, 200 Shepherds Bush Road, London W6 7NL, United Kingdom

<sup>8</sup> EADS Deutschland GmbH, Innovation Works, D-81663 Munich, Germany

## I. Introduction

Since noise originating from the engine or structural vibrations of the chassis has been drastically reduced over the last years, flow induced noise phenomena within the air conditioning (HVAC) system of passenger cars have become a more and more important criterion for the level of comfort of the driver and the passengers. A principal sketch of an air conditioning system in a passenger car is shown in Figure 1. Besides the blower, which is one important noise generating part of a HVAC system, a lot of flow-induced noise is caused by obstacles within the air ducts and vents. Those obstacles generate unsteady fluid motions such as separation or increased levels of turbulence which can cause broadband and even tonal noise.

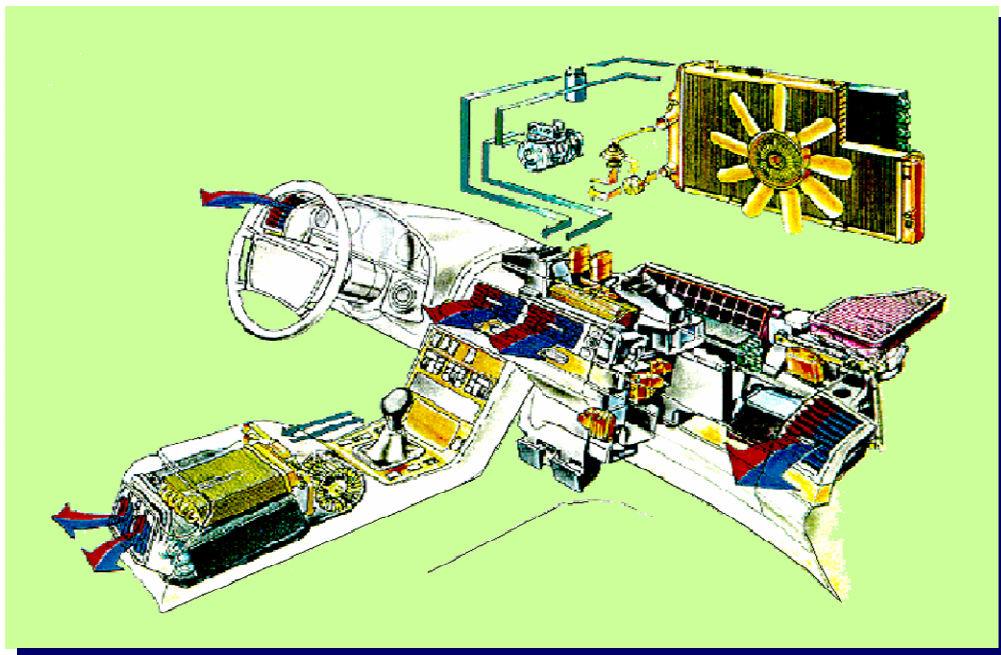


**Figure 1. Sketch of a passenger car HVAC system**

This paper describes ongoing investigations – carried out by a consortium of the German automotive manufacturers Audi, BMW, Daimler, Porsche and Volkswagen in collaboration with the software vendors CD-adapco and Exa – of the feasibility of correctly predicting the noise generated by flaps or other obstacles within air conditioning systems by numerical simulations. Besides that test case dedicated to the noise within HVAC systems, the consortium worked on a second test case dedicated to the phenomenon of sunroof buffeting. Results on that second test case can be found in References 1 and 2.

A correct prediction of flow induced noise phenomena within HVAC systems by numerical simulations would be a major improvement for the development of silent HVAC systems for mainly two reasons. First, numerical simulations can give an insight into the mechanisms of noise generation that can not easily be addressed by experiments. Second, numerical simulations can be used in an early design phase, where no hardware is available. Earlier investigations on aeroacoustic simulations in HVAC systems using commercial codes were for example conducted by Behr<sup>3</sup> and Valeo within the DESTINY projects.

The test case for the present study is a 90° bend with a rectangular cross section. Two different configurations for this test case are studied, one with a flap inside the duct and one without a flap. For this test case, carefully designed experiments as well as carefully designed simulations based on the experiences made in earlier projects by all partners were performed.

## II. Experimental Investigation

Our target was to design an experiment with a radically simplified representation of a HVAC duct geometry that includes important characteristic elements of a real HVAC duct namely pressure driven flow separation and flow around an obstacle. By keeping the geometry as simple as possible we tried to assure that adequate spatial resolution could be realized in the computational studies at least in the sensitive regions. We also intended to define an experimental setup that provides flow conditions at the inflow boundary of the computational domains that could be modelled by steady turbulent inflow conditions.

### A. Simplified HVAC duct

The duct has a 90° bend and a rectangular cross section. The bend causes a pressure-driven flow separation. The obstacle was realized with a simplified throttle flap. Two different configurations were studied: one with a flap inside the duct and one without the flap. Figure 2 shows the geometry of the simplified HVAC duct (all dimensions are measured in mm).

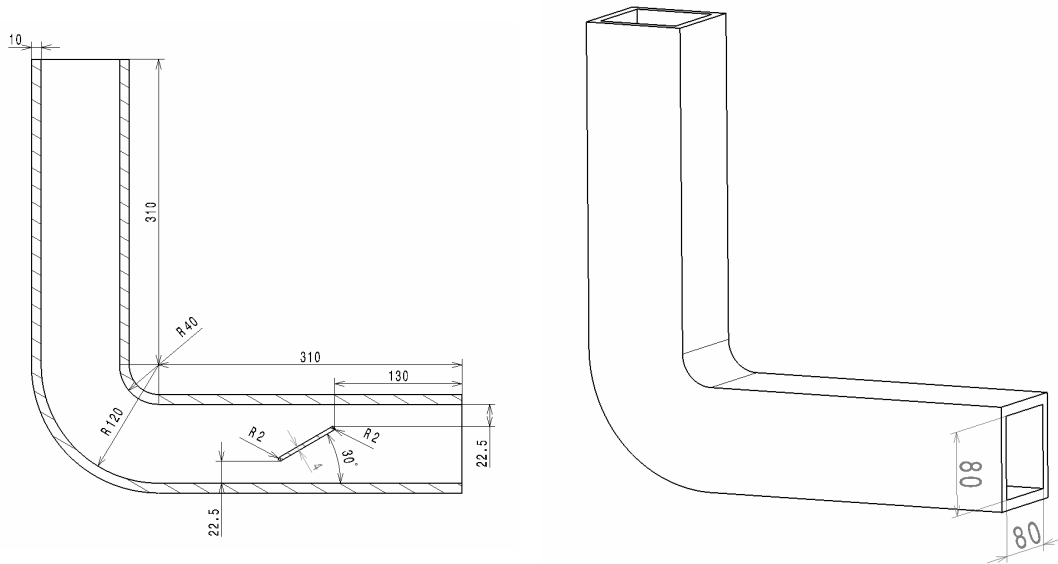


**Figure 2. Geometry of the simplified HVAC duct; left: section cut, right: perspective view**

Two different ducts of identical geometry were used during the experiments: An aluminum duct for microphone measurements and an acrylic glass duct for PIV measurements.

### B. Experimental Setup

An averaged inlet speed of 7.5 m/s was applied within the experiments. It was expected that the simplified HVAC duct generates relatively low sound pressure levels at that flow velocity. Therefore it had to be ensured that the flow noise was not disturbed by background noise of other experimental components. Figure 3 shows the experimental setup.

The flow in the simplified HVAC duct was driven by a variable speed fan that works with very high rotational speeds causing fundamental fan frequencies of more than 1000 Hz. Two mufflers in a tandem configuration efficiently reduced the fan noise. An adapter allowed the smooth transition from the circular cross section of the

mufflers to a quadratic cross section (80\*80 mm). At the downstream end of the adaptor a tripping ridge with a height of 1.5 mm was circumferentially installed.

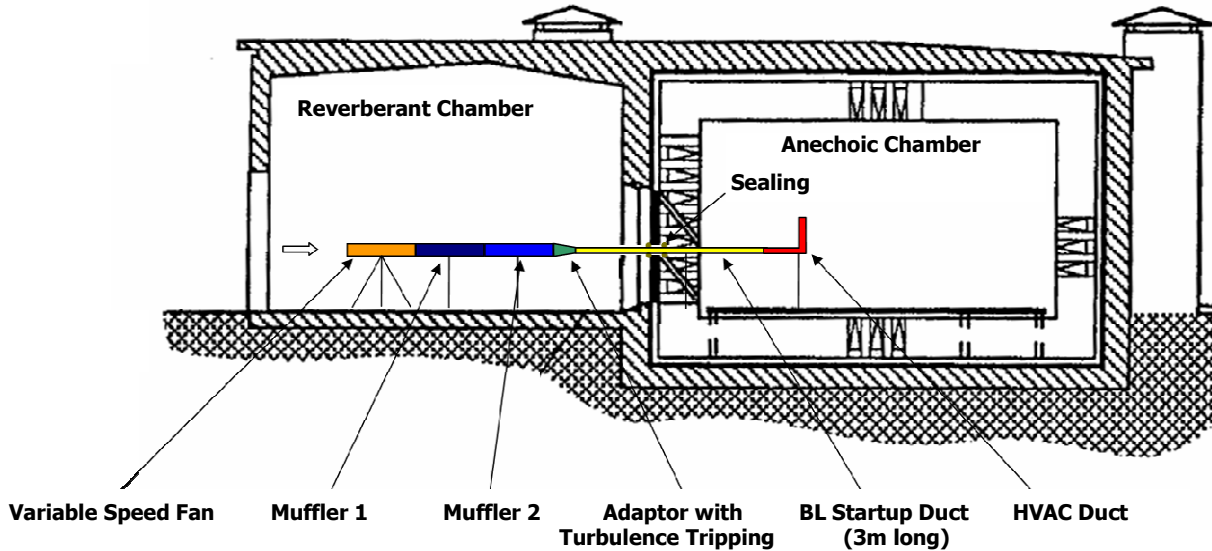


**Figure 3. Experimental Setup**

To ensure a fully developed turbulent flow in the computationally analyzed geometry, a startup duct with 3 m length was attached to the adaptor. The startup duct penetrated a wall between an anechoic and a reverberant chamber. Measurements with a flush mounted microphone at the end of that startup duct proved that tonal fan noise was fully absorbed by the mufflers. The simplified HVAC-duct finally completed the line-up. That experimental setup was installed in two different ways: Fan and mufflers in the anechoic chamber were used to measure the radiated acoustic power in the reverberant chamber, fan and mufflers in the reverberant chamber were used for PIV-, wall pressure fluctuation- and far field noise measurements in the anechoic chamber.

The flow speed in the duct was controlled by adjusting the fan speed. Calibration measurements for flow rate adjustment were undertaken at the end of the startup duct using a traversed hot wire probe and a pressure probe (pitot tube). Different calibration curves were necessary for the cases with and without flap.

### C. Wall Pressure Signal Analysis

Unsteady wall pressure fluctuations were measured at 7 positions within the HVAC duct by means of wall flush mounted  $\frac{1}{4}$  inch microphones. The locations of the microphones are shown in Figure 4, all microphones were mounted in the symmetry plane of the duct. Three pairs of microphones (2&3, 4&5, 6&7) were used to observe local gradients along the walls and also for phase correlation analysis.

In the relevant frequency range a signal-to-noise ratio of more than 20 dB was observed for all wall flush mounted microphones.

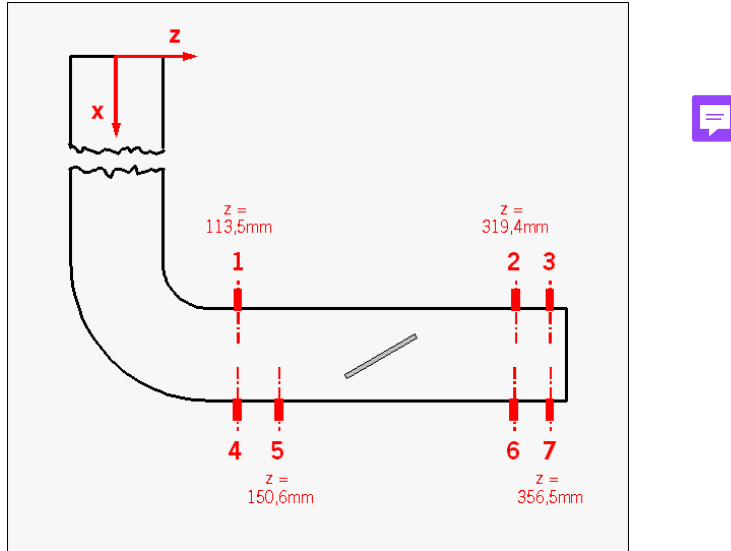


**Figure 4. Positions of the 7 flush mounted microphones to measure wall pressure fluctuations**

The time step that was used for the data sampling in the experiment was not identical to the time step used in the simulations. To be able to compare the experiment with the simulations on a basis of a frequency analysis, all signals therefore had to be resampled. For this resampling, a sampling rate of 2084 Hz was used. All frequency analysis were done on the basis of an FFT using the following parameters:

- DFT-length: 512
- Window: Hanning
- Overlap: 50%
- Frequency resolution: 4 Hz

The sampling rate together with all other parameters lead to a frequency resolution of 4 Hz. All other analysis parameters are summarized in Table 1. The data analysis for the wall pressure signals was done using the software ARTEMIS 8.00 developed by HEAD Acoustics.

	flap			no flap		
	Experiment	PowerFlow	STAR-CD	Experiment	PowerFlow	STAR-CD
<b>Time Data</b>						
phys. time [s]	20.80	0.77	1.01	20.80	0.79	1.50
time step [s]	1.95E-04	2.69E-06	4.00E-05	1.95E-04	1.55E-05	4.00E-05
samples	106496	286077	50500	106496	50910	75000
sample rate [Hz]	5120	371528	50000	5120	64443	50000
<b>Signal Conditioning</b>						
resample	2048	2048	2048	2048	2048	2048
samples for analysis	42598	1577	2068	42598	1618	3072
<b>Signal Analysis</b>						
typ	FFT	FFT	FFT	FFT	FFT	FFT
averages	164	4	6	164	4	10

**Table 1: Parameters for data analysis of wall pressure signals**

#### D. Particle-Image Velocimetry

For a validation of the time averaged flow structures, computed by the two different CFD codes, PIV measurements were conducted inside the HVAC duct. The PIV measurement system consists of the following components:

- Laser (type: New Wave Gemini PIV 15, double pulsed Nd:YAG, 2x 120 mJ, wavelength 532 nm)
- Light Sheet Optics (creates a thin light plane)
- CCD-Camera (type: LA Vision Flow Master 3s)
- Timing Controller (for laser and camera)
- Software
- Seeding generator (type: PIVTEC 40)

For reasonable results the flow medium was seeded with oil droplets made by a mixture of polyethylene glycol and water used in a seeding generator. The basic technique is to take two images shortly after each other and to calculate the distance the particles travelled within 3 - 5 ns time of laser pulses. Cross correlation of two pictures gives exact information about the direction of a particle's movement because it is known which frame was taken first and which one second. The postprocessing and evaluation of all pictures was done with Dantec's FlowManager Software (version 4.71). To increase the signal to noise ratio an averaged background picture has been subtracted from all images before the standard evaluation process was started. Around 100 vector images were averaged to get the final result.

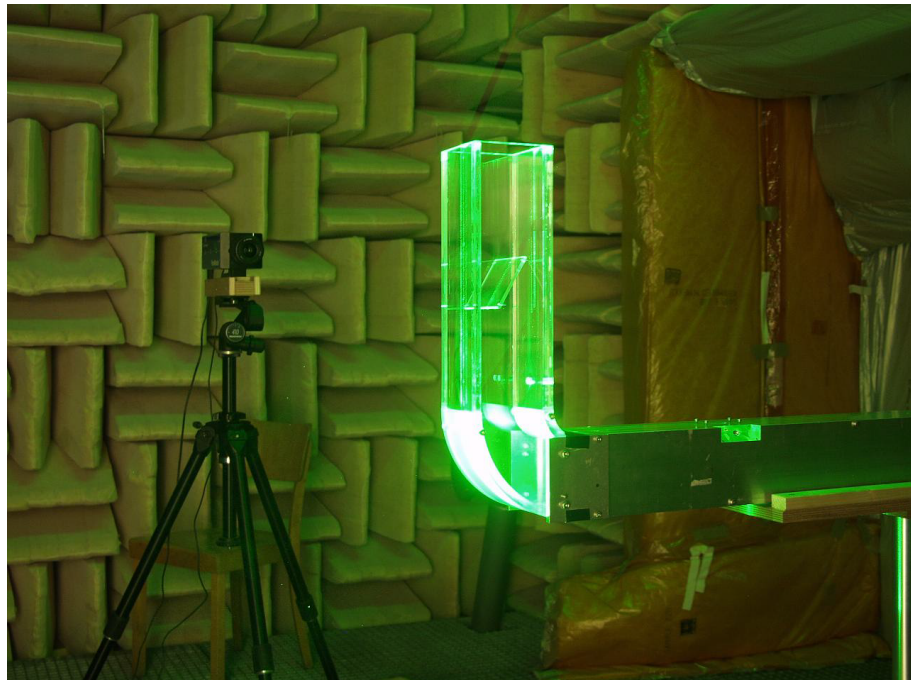
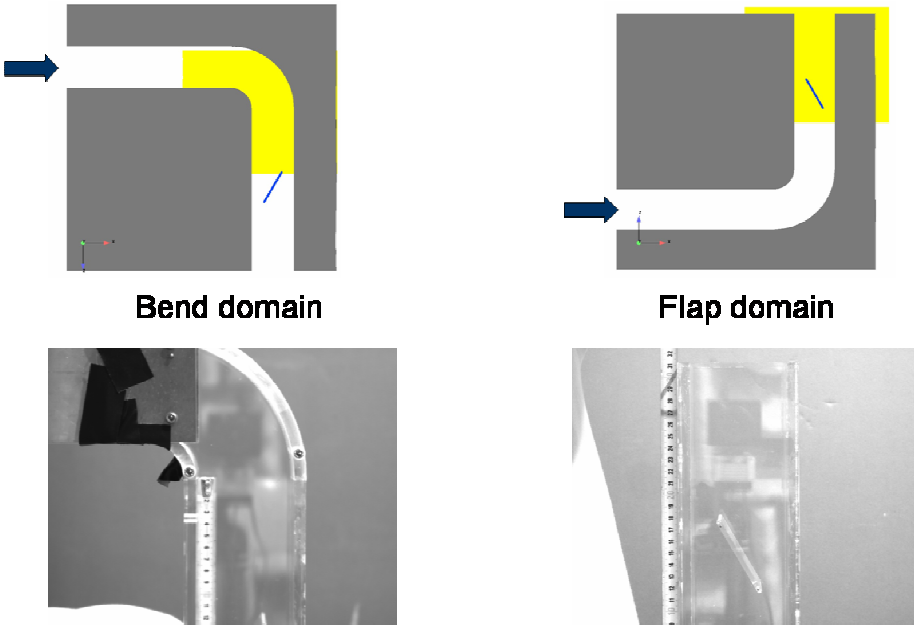


Figure 5. PIV measurement setup

All PIV measurements on the test case were performed with a 2D PIV system. The experimental setup was changed several times to get best results with minimized errors caused by reflections or shadowing effects. To get 3D information it is necessary to run a horizontal and a vertical light sheet plane. If information in the time or frequency domain is needed, further investigation with hot wire anemometry should be performed.

The PIV measurements were performed in the middle plane of the duct ( $y=0$ ) in two different measurement areas to be able to measure within the complete duct starting from the bend, covering the flap region and ending at the duct outlet. The two measurement areas are shown in Figure 6.



**Figure 6. PIV measurement areas**

### III. Numerical Simulations

The test case for the validation of the applicability of numerical simulations to predict the aeroacoustic behavior of the flow within components of a passenger car HVAC system was chosen to have a rather simple geometry. The reason for this choice was that the meshing effort to generate the simulation grids should be kept minimal and that the cell count of the computational grids should be kept in reasonable bounds to also keep the necessary computation times within reasonable bounds. Despite the simple geometry, the test case shows a rather complex three-dimensional flow field, which is representative for flow structures occurring in real life HVAC system components.

The two different configurations (with and without flap) were chosen to evaluate whether the two simulation tools are capable of predicting the change of the aeroacoustic behavior of the flow correctly.

#### A. Simulation Methodology

##### 1. Finite-Volume Simulations (STAR-CD)

The finite volume methodology<sup>4,5</sup> is fully unstructured and employs second-order discretization practices in space and time. A segregated pressure-based solver uses an ideal-gas formulation consistent with compressible flows even in low Mach numbers. It captures the propagation of pressure waves at the local speed of sound and therefore resolves to second-order accuracy any interaction between the fluid dynamics and acoustics. Appropriateness for aeroacoustics simulations is enhanced through the use of non-reflective boundary treatments to eliminate artificial reflections at inlets and pressure boundaries.

Turbulence is modeled through the  $k-\varepsilon$  manifestation of DES (Detached Eddy Simulation)<sup>6</sup>. For the RANS mode underlying DES in these simulations, the near-wall mesh resolution satisfies the best practices for wall-functions ( $y+$  approximately 20) in attached flow regions, whereas a  $y+$  insensitive wall-function formulation is used together with low-Re  $k-\varepsilon$  near-wall damping, appropriate for the separated flow downstream of the right-angle bend and flap. For DES in LES mode, the advection scheme switches to fully centered second-order discretization so as to preserve the convection of large eddy structures.

The geometry downstream of the nozzle is modeled as depicted in Figure 3. This includes the 3m-duct upstream of the test section. It removes the need for experimental data at the inflow boundary since the upstream flow can be assumed to be uniform, evolving towards fully-developed by the end of the 3m section. Modeling the configuration in this way allows for cross-verification of the prediction and measurements at the section  $x=0.0$  upstream of the bend. The flow in the 3m upstream duct is ostensibly steady, therefore the profile at the  $x=0.0$  section needs to be predicted only once, then can subsequently be imposed for any further case configurations both with and without the flap to reduce computational time.

Downstream of the flap, the opening of the 80 mm square duct into the plenum volume is explicitly modeled. Ambient pressure conditions are imposed at the boundaries of the plenum volume placed at least 1.3 m away from the opening. The total mesh count is approximately 2.5 million for both the flap and no-flap cases, with cells refined down to 1 mm in the region downstream of the bend and in the region of the flap. The volume distribution is depicted in Figure 7.

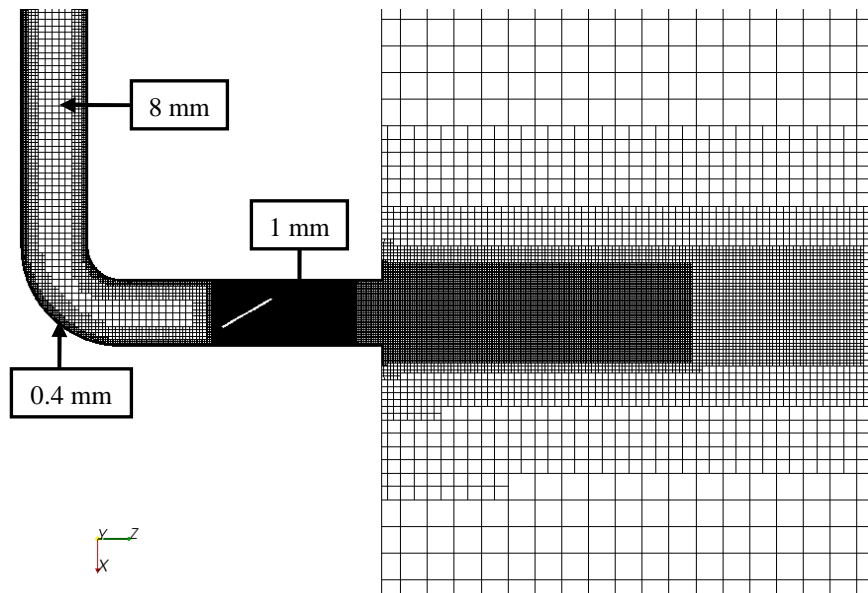


**Figure 7. Volume Distribution in STAR-CD calculations**

Various time steps sizes were assessed and time-step independence confirmed for a range corresponding to a field maximum convective Courant number in the range 1-10. Two seconds of computational time are required to evolve the transient flow towards pseudo-steady limit cycling (0-1sec) and thereafter to gather the statistics (1-2sec). The results presented here are for  $\Delta t=4e-5$  sec, (max. Convective courant number ~4). At this time-step size, 1 second of computational time takes 5.4 days on 16 x 2.8GHz processors.

## 2. Lattice-Boltzmann Simulations (PowerFLOW)

The CFD/CAA code PowerFLOW used is based on the Lattice-Boltzmann Method (LBM<sup>7,8</sup>). Unlike conventional methods based on solving the macroscopic continuum equations as PDE's on a computational grid, the LBM starts from a "mesoscopic" level kinetic equation based on the Boltzmann equation for the particle distribution function, and correct macroscopic fluid dynamics is obtained as a result of evolving the underlying particle distributions. Details of the numerical scheme, including the fundamental LBM dynamical equation, wall boundary conditions, and turbulence modeling, are identical to those given in Ref. 9, Ref. 10 and Ref. 11 and thus are not repeated here. By recovering the compressible Navier-Stokes equations, including an ideal gas equation of state, LBM also inherently recovers acoustics. When sound waves are important, such as problems with coupled aerodynamics and acoustics, the simulated flow must have the same Mach number as the physical conditions, i.e., the ratio of flow speed to sound speed must be the same. Sound wave dissipation occurs due to the bulk viscosity of the LBM scheme, which like the shear viscosity is controlled by the relaxation time<sup>12,13</sup>.

Numerical simulations were done in the aero-acoustics digital environment of PowerFLOW. A detailed CAD model with a well facetized triangular surface mesh was used to specify the geometry (rectangular duct and flap). The inlet section was extruded to a length of 9 m (see Figure 8) and a constant inlet velocity of 7.5 m/s is prescribed at the beginning. An acoustic sponge zone<sup>14</sup> (very high viscosity fluid) is used for the first 6 m to absorb acoustic pressure fluctuations. The next 3 m section uses standard wall and fluid properties consistent with the physical experiment. The velocity profile and the turbulence intensity profile are developed during the simulation. The outlet is defined as a half where all walls are defined as "non-reflective" pressure boundary conditions<sup>15</sup>. The resolution scheme is indicated in Figure 8. The elbow section of the duct is resolved with 1.6 mm voxels while at the inner bend and also around the flap 0.8 mm voxels were used to account for the generation of fine scaled hydrodynamic fluctuations. The simulations were run for about 1.0 second of simulated physical time. For the study presented here the usage of 32 processors is typical, leading to a run time of 1200 CPU h per second physical simulation time.

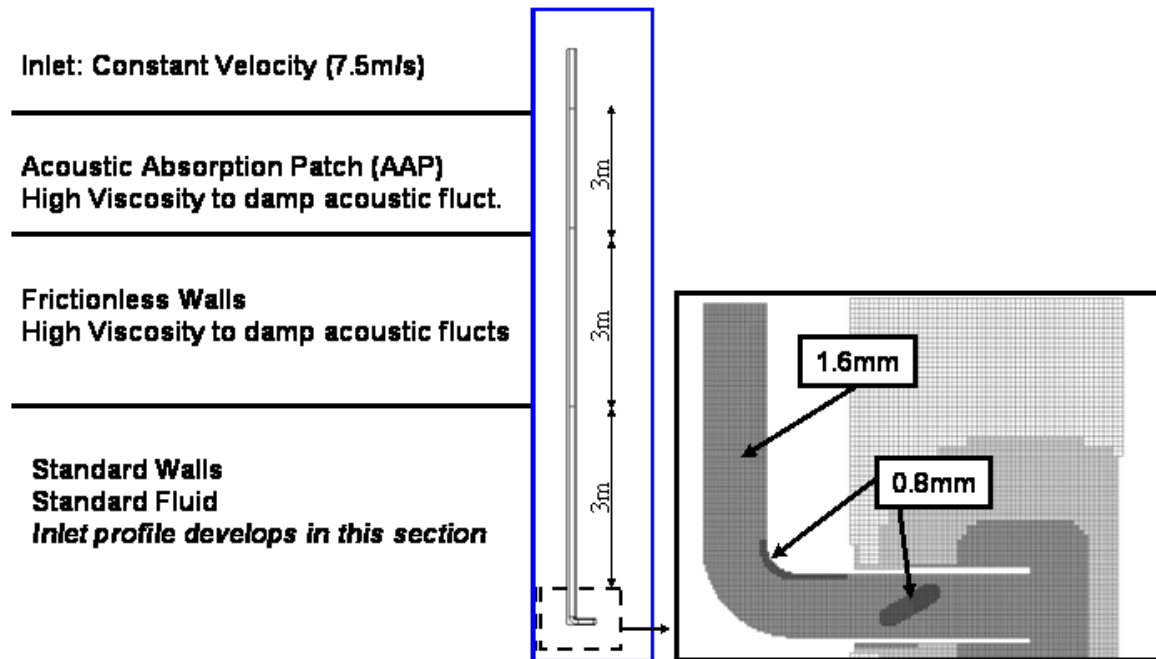


Figure 8. Setup for PowerFLOW calculations

### 3. Summary

The features of the two simulation codes applied in the present study are summarized in Table 2. It can be seen that both apply current state-of-the-art technology in use in industrial CFD.

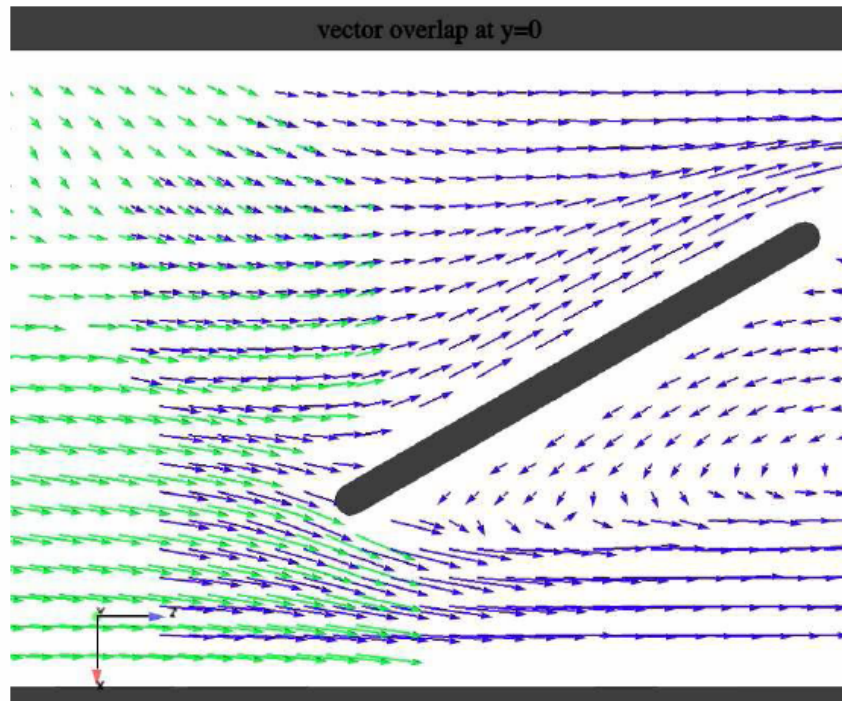
CFD code	STAR-CD	PowerFLOW
Turbulence Model	Detached Eddy Simulation (based on k- $\epsilon$ )	Very Large Eddy Simulation
Temporal Discretization	Crank-Nicholson	n/a (Lattice-Boltzmann)
Time-step size [s]	4e-5	0.38e-5 (finest resolution level)
Simulated Physical time [s]	2.0	1.0
Mesh size	2.4 - 2.7 million	Finest equivalent voxels: 5.4 million Total voxels: 12.4 million
Smallest cell size [mm]	1	0.8
Convective Differencing Scheme	MARS in DES_RANS mode, CD in DES_LES mode	n/a
Computing resources	16 x 2.8 GHz processors	3 GHz Xenon Linux Cluster
Run time [CPU.h / s sim.time]	2100	1200

Table2. Summary of simulation methods

## B. Simulation Results – Comparison with Measured Data

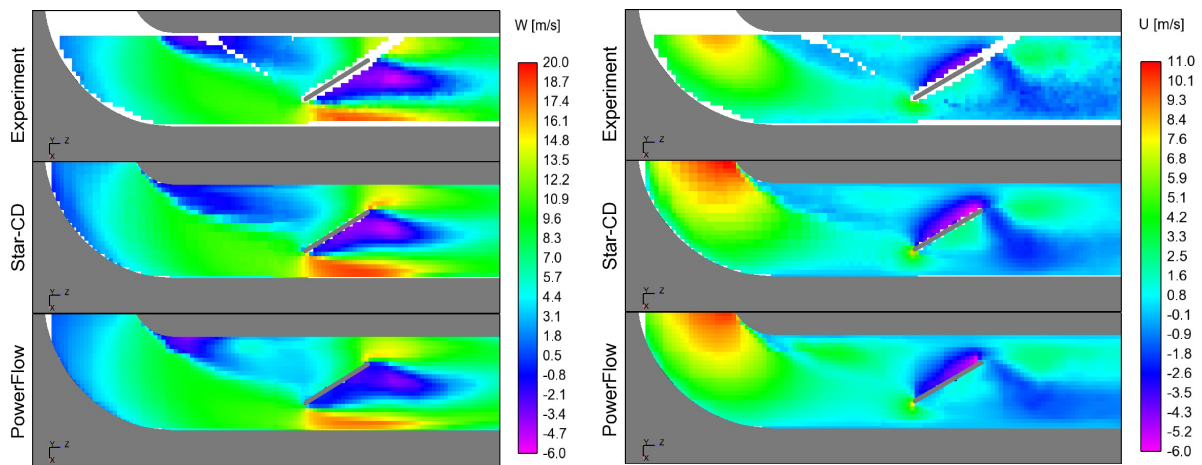
### 1. Time Averaged Flow Field

As described in section II.D, the time averaged flow field within the HVAC duct was measured using a PIV system. For the two different areas that were measured, two different experimental setups were used. The two measurement areas had a small overlapping part covering around 3 cm. This part, where the two measurement areas overlap, gave us the possibility to compare the measurements within the two different setups. This comparison is shown in Figure 9. The velocity vectors measured with the first experimental setup are colored in green, the ones measured with the second setup are colored in blue. In the overlapping region both measurements agree very well, both for the velocity magnitude as well as the flow direction. One should keep in mind for that comparison that the measurement grids of the two PIV measurement setups do not coincide. In the following comparison the measurements of the two different experimental setups are mostly plotted together to be able to show the complete HVAC duct starting from the bend, covering the region of the flap and ending at the duct outlet.



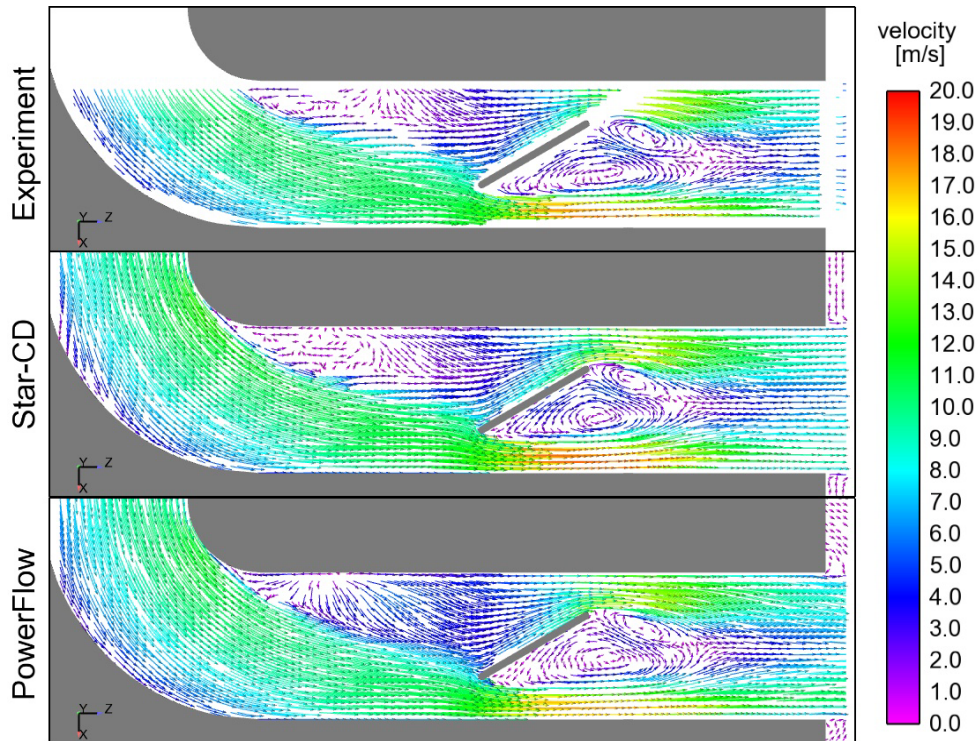
**Figure 9. Comparison of overlapping regions for two measurement setups**

One first comparison is shown in Figure 10 on the left. Here the time averaged velocity component in z-direction in the section  $y=0$  (middle section of the duct) is shown. The PIV measurements (top) are compared to the STAR-CD simulations (middle) and the PowerFLOW simulations (bottom). The first thing that can be recognized are small white spots within the measurement area of the PIV data. Those spots are areas where the PIV results are not reliable. They were caused by optical difficulties occurring in the experimental setup such as shadows or reflections. Besides those white spots, the time averaged flow field of the two simulations fit pretty well to the experiment. For the size and the shape of the separation region behind the flap as well as for the flow field approaching the flap, both simulation tools show a comparable good agreement with the measurements. Differences between the results of the two simulation tools can be found by looking closer into the details of the flow field. These differences will be discussed later.



**Figure 10. Comparison of simulations and experiment: time averaged velocity components in z-direction (left) and x-direction (right) in section  $y=0$**

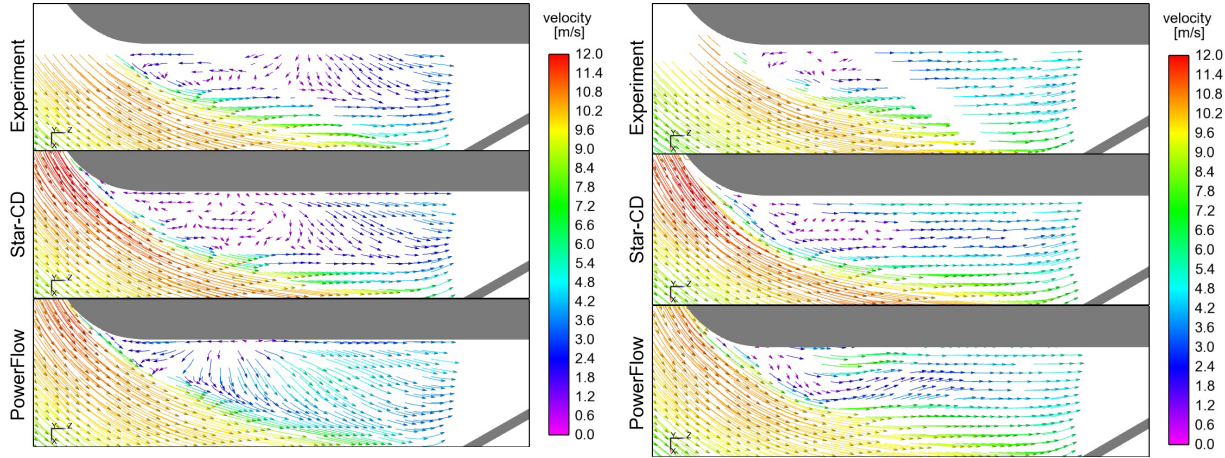
Figure 10 on the right displays the time averaged velocity component in x-direction in the middle section of the duct ( $y=0$ ). Figure 11 shows the projected velocity vectors within this section. Both figures confirm the overall good agreement between the measurements and the two different simulations. As can be noticed within the vector plots, the area where the two measurement setups overlap is not only visible within the PIV data but also within the results of the two simulation tools. This is due to the fact that the simulation results are mapped onto the PIV grid to have a direct comparison between the simulations obtained on different grids and the measurements. Due to the smoothness of the averaged flow field the error caused by this mapping procedure is negligible.



**Figure 11. Comparison of simulations and experiment: projected velocity vectors in section  $y=0$**

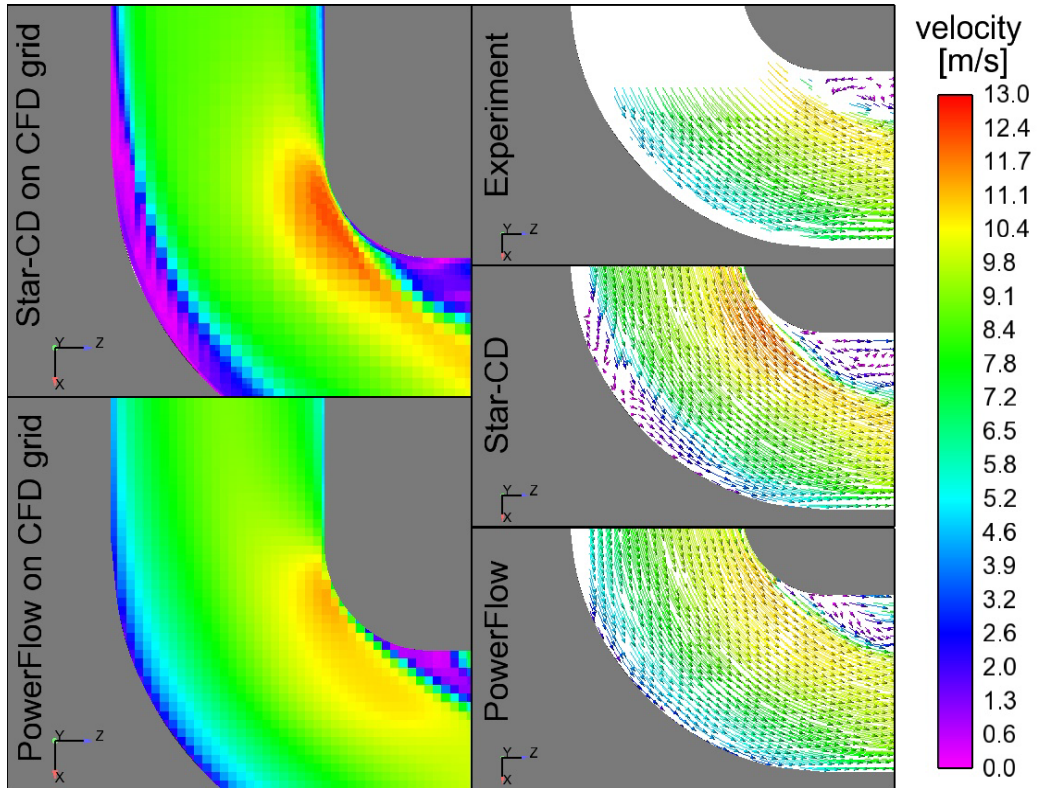
Some discrepancies between simulations and experiments can be found in the small separation region at the inner radius of the bend (especially for PowerFLOW) and in the region of the outer radius of the bend (especially for

STAR-CD). Figure 12 shows a closer look at the small separation region at the inner radius. Additional to the section plot at  $y=0$  a section plot at  $y=0.02$  m (at 1/4th of the duct width) is shown.



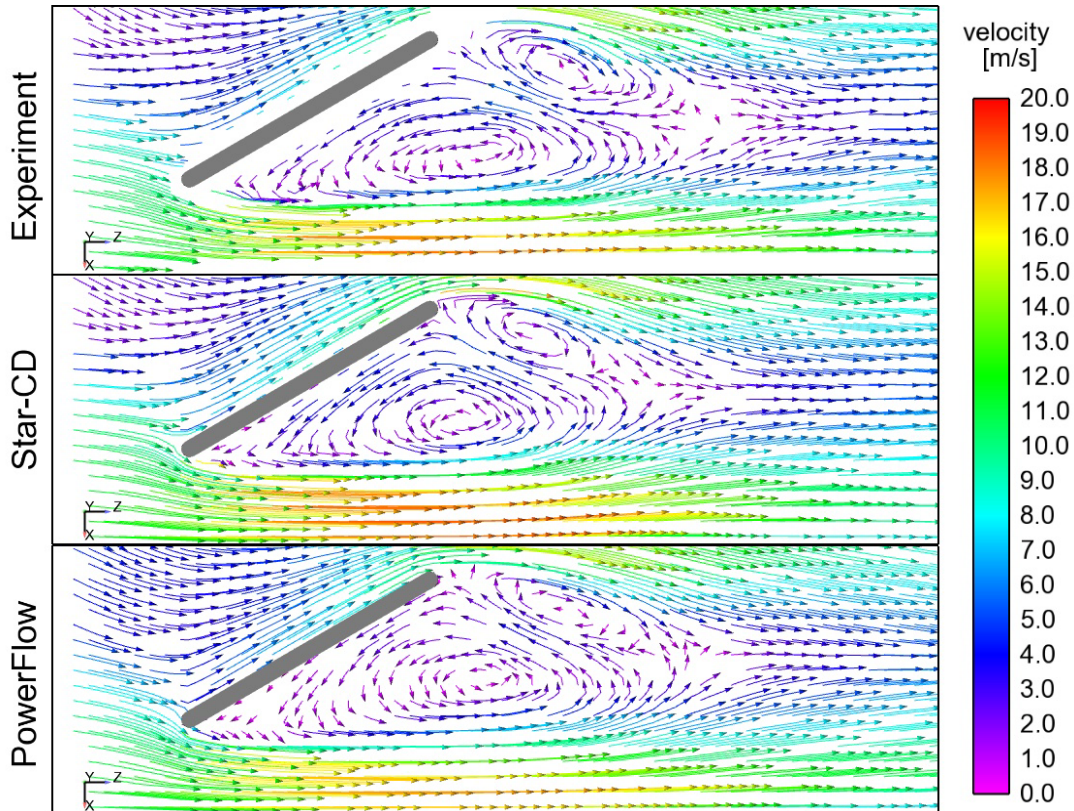
**Figure 12. Comparison of simulations and experiment: projected velocity vectors in section  $y=0$  (left) and  $y=0.02$  m (right)**

The two plots illustrate that in the PowerFLOW simulation the separation region is calculated too small and that downstream of the separation the acceleration of the flow is faster than in experiment. The STAR-CD simulation in contrast shows a tiny separation zone at the outer radius of the bend that is not visible in experiment (see Figure 13). This separation mainly appears off-centre from the middle section of the duct.



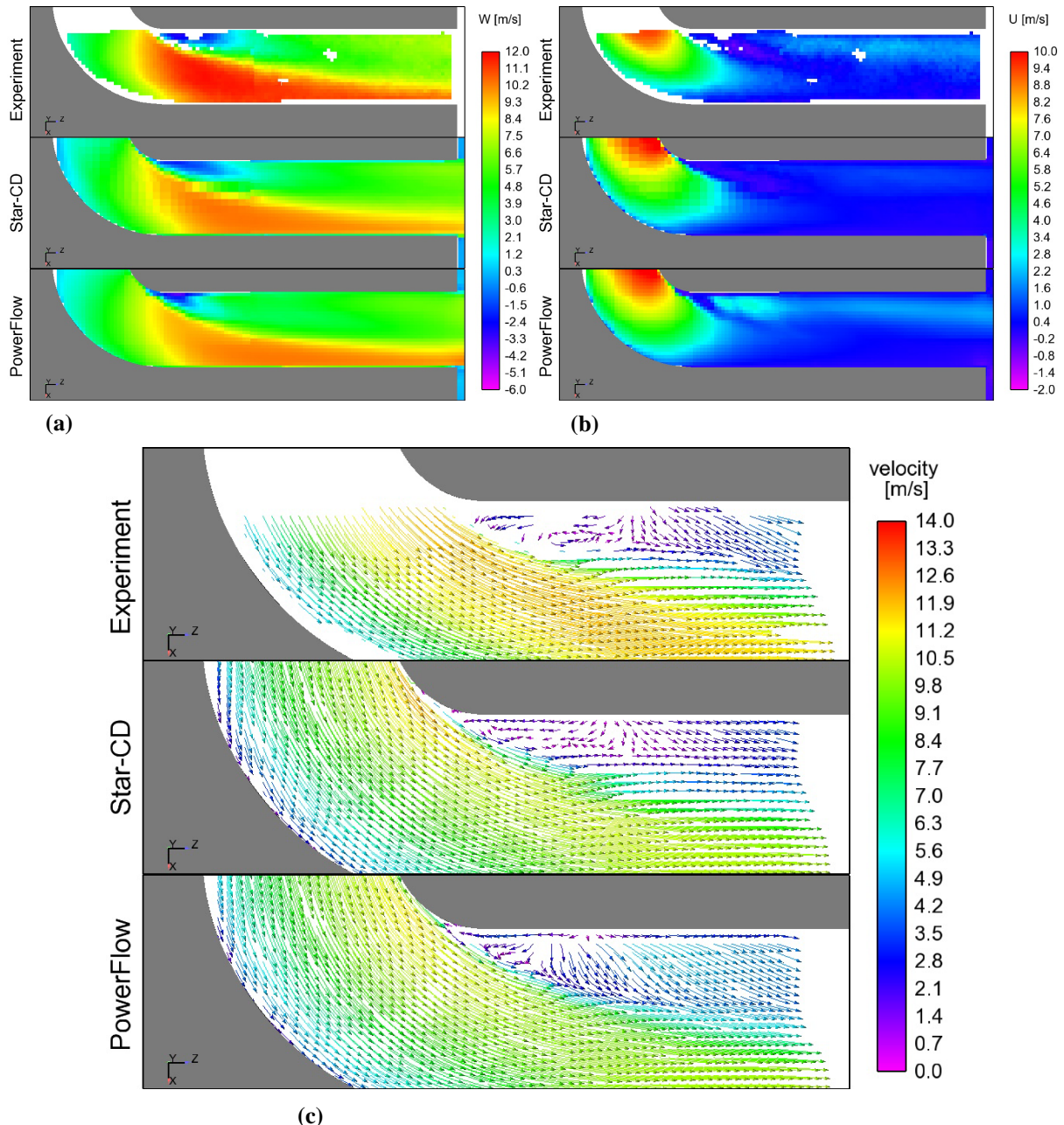
**Figure 13. Comparison of simulations and experiment: projected velocity vectors in section  $y=0.02$  m, close up view of outer bend radius**

Figure 14 shows a detailed view of the flow in the vicinity of the leading edge of the flap. This is a critical area for a correct modeling of the noise generation for this test case. Even if the agreement of the two simulations with the experiment is not perfect, it is hard to evaluate remarkable differences between them. Especially the angle of attack of the flow to the flap leading edge as well as the velocity magnitude in the region of the leading edge are very well predicted by both simulation tools. This shows the high quality of the simulation results that was achieved in the course of this project.



**Figure 14. Comparison of simulations and experiment: projected velocity vectors in section  $y=0$ , close up view of flap leading edge**

Finally, Figure 15 shows comparisons between the simulations and the experiment for the configuration without flap. What can be seen is that the time averaged velocity component in z-direction is on average a little bit higher in the experiment than in the simulations. It was not possible to clearly identify the reason for this behavior. One possible explanation is that the mass flow in the experiment was slightly higher than in the simulations. Besides that small discrepancy, the overall flow field predicted by the two CFD codes looks quite similar compared to the experiment. Differences can again be found by looking into the details. Since those differences in the details of the flow field are comparable to the ones discussed in detail for the configuration with flap, a further discussion of them will be skipped.



**Figure 15. Comparison of simulations and experiment for configuration without flap in section  $y=0$ :** (a) time averaged velocity component in  $z$ -direction, (b) time averaged velocity component in  $x$ -direction, (c) projected velocity vectors

## 2. Unsteady Flow Phenomena

Figure 16 shows a comparison between the experiment and the two simulations for the case with the flap. Plotted are the unsteady wall pressure fluctuations at three microphone positions versus frequency.

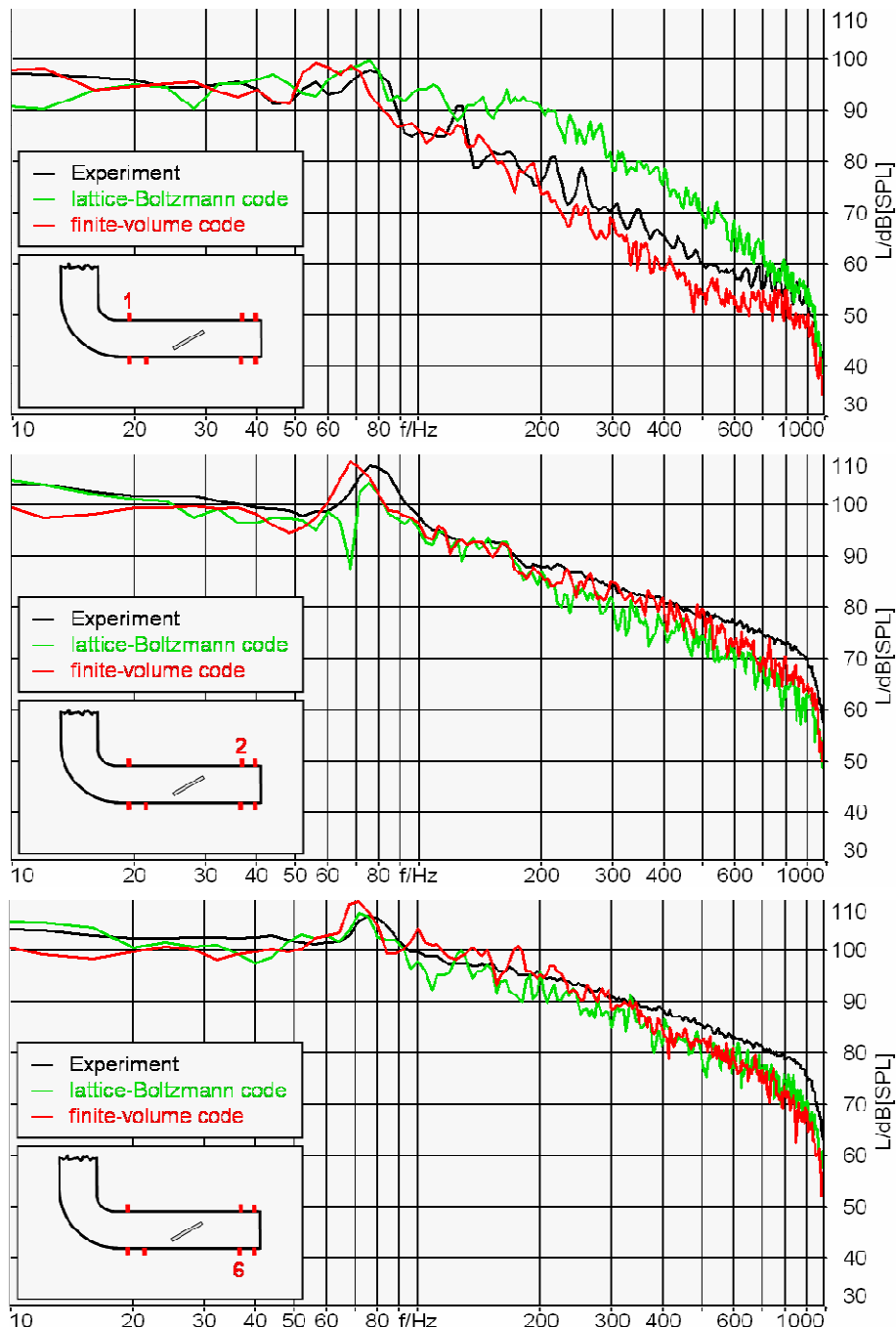


**Figure 16. Comparison of experiment and simulations: Wall pressure signals at microphone positions for the case with flap**

The overall agreement is good for both CFD codes (PowerFLOW as well as STAR-CD). The amplitude of the pressure fluctuations fits well to the experiment for all microphone positions. The hump in the spectrum that can be seen in the experiment at around 80 Hz is also predicted with an acceptable accuracy by both CFD codes. Small differences between the two CFD codes can be found by looking into the details. For STAR-CD the hump seems to be shifted a little bit towards a lower frequency, whereas for PowerFLOW the hump is not really pronounced for microphone position 2.

Figure 17 shows the comparison of the unsteady wall pressure signals for the case without the flap.

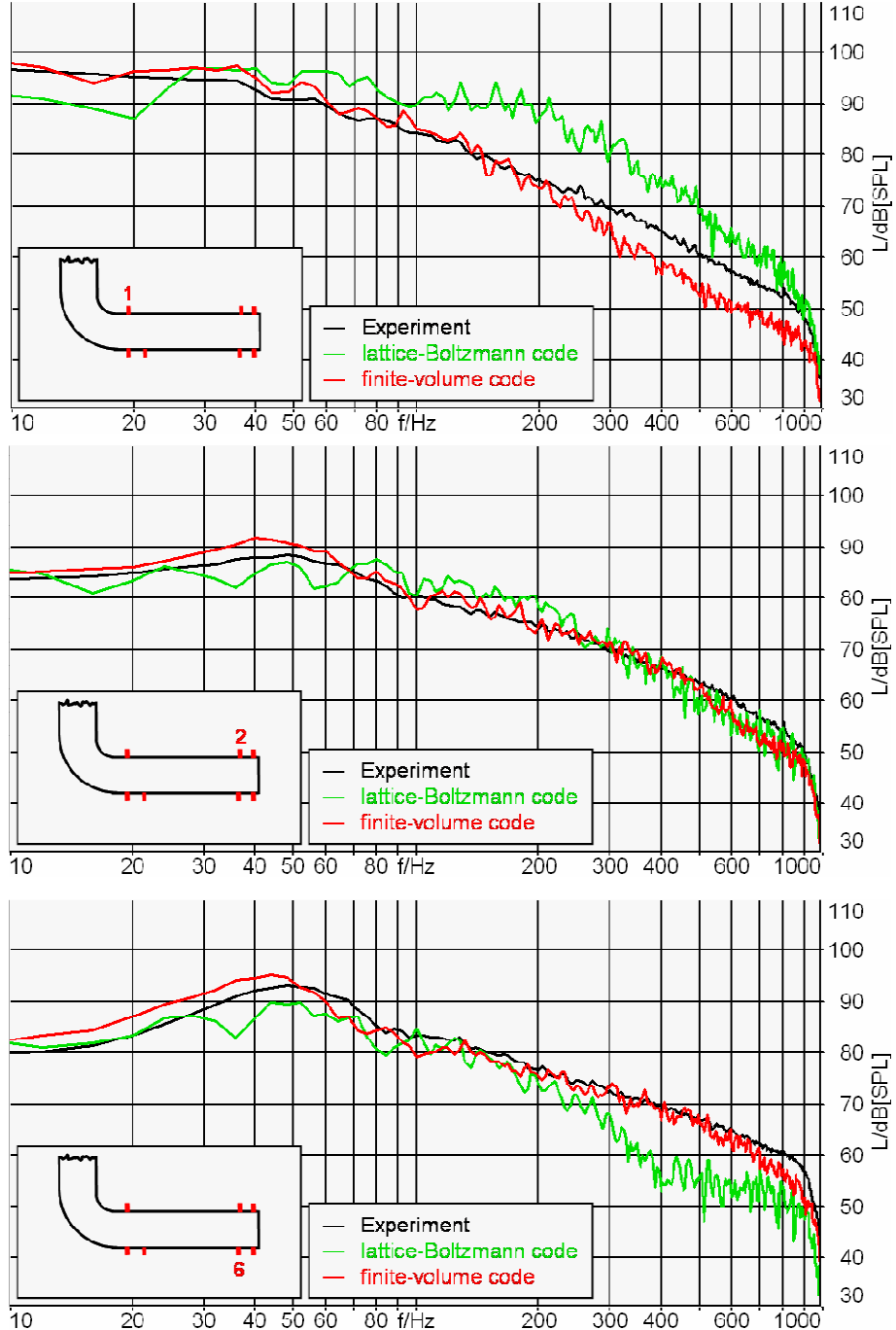


**Figure 17: Comparison of experiment and simulations: Wall pressure signals at microphone positions for the case without flap**

The agreement of the results of the two CFD codes is comparably good than for the case with the flap. Considerably higher discrepancies can be found between the PowerFLOW results and the experiment at microphone position 1 and at microphone position 6 above 300 Hz.

## IV. Conclusions

In the present paper a detailed validation study for the first step of a two step approach for aeroacoustic simulations within components of HVAC systems in passenger cars is shown. This first step consists of an unsteady CFD simulation. For a simplified HVAC duct results obtained with two different commercial CFD codes (STAR-CD and PowerFLOW) were compared to experimental measurements. Both codes show a good agreement to the measurements for time averaged flow structures as well as for wall pressure fluctuations. Differences between the two codes could be found by having a closer look into the details of the flow field. This validation study has shown that both codes are capable of accurately predicting the unsteady flow structures within HVAC components that are the sources for the aerodynamically generated noise.

The next step for a complete aeroacoustic simulation of noise generated in HVAC systems would be to calculate aeroacoustic sources from the results of the unsteady CFD simulations, to feed them into an acoustic code and to calculate the propagation of the sound from the generation area to an observer position. This work has already been started also as a detailed validation study but is still ongoing.

## Acknowledgments

The authors wish to thank D. Freed (Exa Corp.) for his valuable support in carrying out the PowerFLOW work, as well as C. Fertl and M. Höll (BMW AG) for performing 2D PIV measurements reported here.

## References

- <sup>1</sup>Islam M. et al., "Investigations of Sunroof Buffeting in an Idealised Generic Vehicle Model – Part I: Experimental Results", AIAA 2008-2900, 2008
- <sup>2</sup>Islam M. et al., "Investigations of Sunroof Buffeting in an Idealised Generic Vehicle Model – Part II: Numerical Simulations", AIAA 2008-2901, 2008
- <sup>3</sup>Brotz F. et al., "Aeroacoustic CFD Simulation for Automotive Air Conditioning Applications: Behr's Experience", VMTS 8, 2007
- <sup>4</sup>Mendonça F., chapter on "Industrial Aeroacoustics Analysis" in *LES for Acoustics*, ed. Wagner, Hutt and Sagaut, ISBN-13:9780521871440, Cambridge University Press, 2007
- <sup>5</sup>STAR-CD Methodology Manual, CD-adapco [www.cd-adapco.com](http://www.cd-adapco.com)
- <sup>6</sup>Allen, R., Mendonça, F., and Kirkham, D., "RANS and DES turbulence model predictions of noise on the M219 cavity at  $M=0.85$ ", International Journal of Aeroacoustics, Volume 4, Numbers 1-2, Jan 2005
- <sup>7</sup>Wolf-Gladrow, D., "Lattice-Gas Cellular Automata and Lattice Boltzmann Models", Springer Verlag, Germany, 2000.
- <sup>8</sup>Bhatnagar, P., Gross, E. and Krook, M., "A model for collision processes in gases. I. small amplitude processes in charged and neutral one-component system", Phys. Rev., vol.94, pp.511-525, 1954.
- <sup>9</sup>Chen, H., "Volumetric Formulation of the Lattice Boltzmann Method for Fluid Dynamics: Basic Concept", Phys. Rev. E, Vol. 58, pp. 3955-3963, 1998.
- <sup>10</sup>Chen, H., Teixeira, C., Molvig, K., "Realization of Fluid Boundary Conditions via Discrete Boltzmann Dynamics," Int'l. J. Mod. Phys. C, 9 (8), p. 1281, 1998.
- <sup>11</sup>Chen, H., Orszag, S., Staroselsky, I. and Succi, S., "Expanded Analogy between Boltzmann Kinetic Theory of Fluid and Turbulence", J. Fluid Mech., Vol. 519, 2004, pp. 307-314.
- <sup>12</sup>Crouse, B., Senthooran S., Balasubramanian G., Freed, D., Karbon, K., "Computational Aeroacoustics Investigation of Automobile Sunroof Buffeting", SAE-paper 2007-01-2403, 2007.
- <sup>13</sup>Crouse, B., Freed, D., Balasubramanian, G., Senthooran, S., Lew, P.-T., Mongeau, L., "Fundamental Aero-Acoustic Capabilities of the Lattice-Boltzmann Method", AIAA 2006-2571, 2006.
- <sup>14</sup>Exa internal document, 2007
- <sup>15</sup>Exa internal document, 2004